

# Plasma screening of nuclear fusion reactions in liquid layers of compact degenerate stars: a first-principle study

D. A. Baiko\*

*Ioffe Institute, Politekhnicheskaya 26, 194021 Saint Petersburg, Russia*

Accepted; Received ; in original form

## ABSTRACT

A reliable description of nuclear fusion reactions in inner layers of white dwarfs and envelopes of neutron stars is important for realistic modelling of a wide range of observable astrophysical phenomena from accreting neutron stars to type Ia supernovae. We study the problem of screening of the Coulomb barrier impeding the reactions, by a plasma surrounding the fusing nuclei. Numerical calculations of the screening factor are performed from the first principles with the aid of quantum-mechanical path integrals in the model of a one-component plasma of atomic nuclei for temperatures and densities typical for dense liquid layers of compact degenerate stars. We do not rely on various quasiclassic approximations widely used in the literature, such as factoring-out the tunneling process, tunneling in an average spherically symmetric mean-force potential, usage of classic free energies and pair correlation functions, linear mixing rule and so on. In general, a good agreement with earlier results from the thermonuclear limit to  $\Gamma \sim 100$  is found. For a very strongly coupled liquid  $100 \lesssim \Gamma \leq 175$ , a deviation from currently used parametrisations of the reaction rates is discovered and approximated by a simple analytic expression. The developed method of nuclear reaction rate calculations with account of plasma screening can be extended to ion mixtures and crystallised phases of stellar matter.

**Key words:** dense matter – nuclear reactions, nucleosynthesis, abundances – stars: interiors – (stars:) white dwarfs – stars: neutron.

## 1 INTRODUCTION

Reprocessing of matter accreted onto a compact degenerate star, a white dwarf or a neutron star, from a binary companion is associated with a number of exciting astrophysical phenomena. The accreted material undergoes a series of nuclear transformations via an extensive network of reactions involving as many as hundreds of isotopes. In some sources, for instance, in soft X-ray transients with transiently accreting neutron stars, this ‘nuclear burning’ proceeds in a quasisteady-state fashion. The reactions occur throughout the accreted crust, slowly alter its composition and properties, determine the thermal state of the whole neutron star, and power its quiescent emission (e.g., [Shchepochin, Gusakov & Chugunov 2021](#), and references therein). In other sources, the reactions may enter a thermal runaway regime and produce spectacular explosions. These include type I X-ray bursts and superbursts from accreting neutron stars as well as novae and, possibly, type Ia supernovae from accreting white dwarfs (e.g., [Parikh, José & Sala 2014](#); [in ’t Zand 2017](#); [Soker 2019](#)).

Mergers of compact stars also achieve extreme physical conditions and trigger large scale nucleosynthesis. A merger of two white dwarfs can be accompanied by a nuclear detona-

tion of the core material which is another channel for a type Ia supernova (e.g., [Ruiter 2020](#)). Alternatively, two white dwarfs may merge into a single massive one with a distinctive composition (e.g., [Jeffery, Karakas & Saio 2011](#)). Lastly, when two neutron stars merge, one anticipates a major transformation of their crustal matter.

In order to model these phenomena and their outcomes realistically, a reliable microphysics is required. In particular, an accurate description of reactions involved seems to be really important. One of the key reaction types are nuclear fusion reactions. Let us consider an element of an outer neutron star crust or of a white dwarf core and assume that there are only fully ionized atoms (i.e. atomic nuclei) and electrons present in this matter element. Then, a pair of neighbouring nuclei may suffer a quantum mechanical tunneling and fuse. A nuclear reaction occurs and new nuclei form. This process results in an energy release and a change of matter composition.

It is well-known that the plasma surrounding the fusing nuclei modifies the fusion probability ([Wildhack 1940](#); [Schatzman 1948](#); [Salpeter 1954](#)). Effectively, other ions push the pair of fusing nuclei towards each other forcing them to be closer and to spend more time near each other thereby enhancing the tunneling probability (e.g., [Ogata 1997](#)). On top of that, the electron density responds to the presence of nuclei and screens the Coulomb force between them (e.g.,

\* E-mail: baiko@astro.ioffe.ru

Potekhin & Chabrier 2013). Thus, the ambient plasma results in a reduction of the Coulomb barrier and an amplification of the reaction rates. These effects are often referred to as plasma screening of nuclear reactions (for reviews, see Yakovlev & Shalybkov 1989; Ichimaru 1993).

The main topic of this paper is the ion contribution to plasma screening which, in spite of extensive studies, is still subject to some theoretical uncertainty. We shall treat electrons simply as a uniform incompressible charge-compensating background. (Current state of the art in the theory of electron screening is summarised in Potekhin & Chabrier 2013, and references therein.) Moreover, we shall limit our study to the plasma with nuclei of only one sort (with the charge number  $Z_i$  and mass  $m_i$ ) deferring a more astrophysically relevant case of multi-ionic mixtures to a future work (see Chugunov & DeWitt 2009, for state of the art in this area). In plasma physics, such a model is known as a one-component plasma (OCP).

From a practical standpoint, one is interested in the rate of nuclear reactions per unit volume at a given temperature  $T$  and density  $\rho$ . It can be written as (e.g., Ichimaru 1993)

$$R = \frac{n_i^2 a_B}{\pi \hbar} S(E_{\text{pk}}) g(0), \quad (1)$$

where  $n_i$  is the ion density,  $a_B = \hbar^2/(m_i Z_i^2 e^2)$  is the ion Bohr radius,  $E_{\text{pk}}$  is the Gamow-peak energy (see also Chugunov & DeWitt 2009) and  $S(E)$  is the astrophysical factor. The latter quantity contains all the information about nuclear aspects of the reaction. For non-resonant reactions, it is a relatively slowly varying function of fusing nuclei energy and, in general, it is not known very precisely (typical uncertainty is a factor of 2–10, e.g., Beard et al. 2010, and references therein). We shall not discuss the astrophysical factors in this work.

Finally,  $g(0)$  is the ion pair correlation function of the plasma at zero separation. It is this quantity which encodes the plasma screening effect and is the main subject of our interest.<sup>1</sup> Clearly, if the plasma were classic,  $g(0)$  would be strictly equal to zero due to the Coulomb repulsion of bare nuclei. In reality though, the nuclei can tunnel through the Coulomb barrier and there is a non-zero (albeit very small) probability for a pair of nuclei to occupy the same spatial point, so that the quantum-mechanical  $g(0) \neq 0$ . If the plasma screening were turned off, the quantum-mechanical  $g(0)$  would be equal to the textbook thermonuclear limit (e.g., Clayton 1983). If the screening is weak, which is the case in the gaseous ion plasma (domain I in Fig. 1), then  $g(0)$  can be deduced from the well-known Debye-Hückel approximation (Salpeter 1954). These limits of almost pure thermonuclear fusion are relevant for ordinary stars, outermost layers of degenerate stars, and for primordial nucleosynthesis in the early Universe.

As one switches to inner layers of compact stars, the screening effect becomes much more pronounced. For applications, one is interested in an intermediate range of physical parameters where the reaction rate  $R$  is neither too big nor too small.

<sup>1</sup> Brown & Sawyer (1997) and Sawyer (2010) have developed a more general theory of plasma screening, which goes beyond Eq. (1). Presently, an application of this theory does not look practical, which makes it hard to gauge its actual impact on nuclear reaction rates.

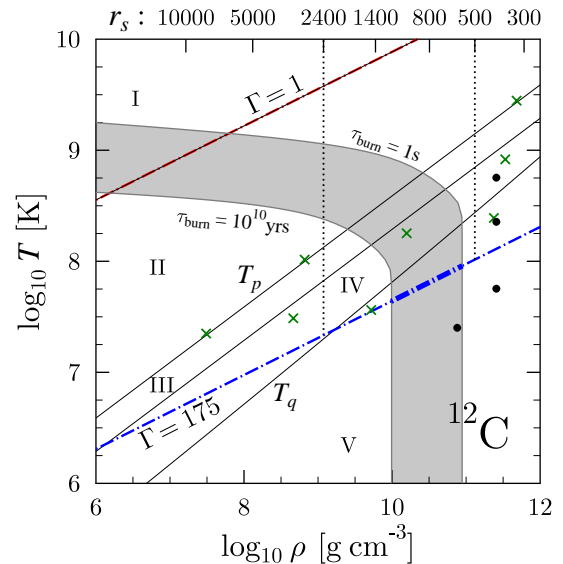


**Figure 1.**  $T$ - $\rho$  plane of fully ionized carbon matter modelled as an OCP. Shaded strip is the ‘relevance strip’, the parameter range across which the burning time  $\tau_{\text{burn}}$  changes from 1 second to  $10^{10}$  years. Roman numerals (I–V) indicate various plasma screening domains, their boundaries are plotted by thin solid lines. Dot-dashed lines show gas-liquid and liquid-solid transitions. Crosses and big dots are positions of datapoints of Ogata (1997) and Militzer & Pollock (2005), respectively. Dotted lines bound the density range where the present calculations are performed. Upper  $x$ -axis is labelled by  $r_s$  values.

Otherwise, either the assumed composition would be unrealistic and heavier nuclei would have to be considered instead, or, by contrast, nothing would be happening in the matter element. Since this is a well-researched problem, the important parameter range is, in principle, already known rather accurately. For carbon plasma, it is shown by a shaded strip in Fig. 1, which is adopted with some modifications from Fig. 1 of Chugunov, DeWitt & Yakovlev (2007).

The strip spans the parameter range where the burning time, defined as  $\tau_{\text{burn}} = n_i/R$ , varies from 1 second to  $10^{10}$  years. The burning time can be phenomenally sensitive to density and/or temperature. For instance, in the high-density (pyncnonuclear) regime in Fig. 1, it changes by 17 orders of magnitude if the density changes by less than an order. This implies that any reasonably anticipated improvements of the reaction rates will result in only barely visible modifications of this practically relevant physical domain (for brevity, we shall refer to this domain as the ‘relevance strip’).

The fact that the strip is shown specifically for carbon plasma does not limit the discussion because the problem for other ions (as long as it is still the OCP model and the nuclear reaction in question is non-resonant) is self-similar and can be solved by simple scaling with the aid of two dimensionless parameters. These are the familiar Coulomb coupling parameter  $\Gamma = Z_i^2 e^2 / (a_i T)$  and the ion density parameter  $r_s = a_i / a_B$ . In this case,  $a_i = (4\pi n_i / 3)^{-1/3}$  is the Wigner-Seitz radius. Let us remind that  $\Gamma = 1$  corresponds to the liquid-gas continuous transition and  $\Gamma = 175$  is the melting phase transition for the classic OCP (e.g., Haensel, Potekhin & Yakovlev 2007). These equations are represented by dot-dashed lines in Fig. 1.

Since the pioneering work of Salpeter & Van Horn (1969),

it has been customary to divide the temperature-density plane into domains corresponding to different plasma screening physics. These are also shown in Fig. 1 and marked by roman numerals (I–V). Their boundaries (as given in Chugunov et al. 2007) are displayed by thin solid lines described by the following equations:  $\Gamma = 1$ ,  $T = T_p$ ,  $T = 0.5T_p$ , and  $T = T_q$ , where  $T_p = \hbar\sqrt{4\pi n_i Z^2 e^2 / m_i}$  is the ion plasma temperature and  $T_q = T_p / \ln(r_s/3)$ . The relevance strip crosses these domains and lines separating gas, liquid, and solid phases in such a way that, in the gas phase, the strip is always in domain I (‘thermonuclear with weak screening’). In the solid phase, it is always in domain V (‘ $T = 0$  pycnonuclear’). In the liquid phase, the strip traverses domain II (‘thermonuclear with strong screening’), intermediate domains III and IV, and domain V.

Thus, the segment of the melting line belonging to the relevance strip (shown by a thicker dot-dashed line in Fig. 1) is completely within the  $T = 0$  pycnonuclear domain V in which the reaction rates are supposedly independent of temperature. This is actually surprising, because melting/crystallisation in such a plasma is certainly a thermal phenomenon. Hence, one tends to expect the temperature dependence of the rates in the liquid to continue all the way down to crystallisation and, to some extent, into the solid phase as well. It is worth to keep this observation in mind when we analyse various results in Sections 3 and 4.

In general, the domain boundaries are deduced from qualitative arguments and should not be taken too literally. For instance, one can find three versions of the upper boundary of the  $T = 0$  pycnonuclear domain in Salpeter & Van Horn (1969): in their Fig. 1, p. 187, and p. 198. For carbon at  $\rho = 3 \times 10^{10} \text{ g cm}^{-3}$  ( $r_s \approx 818$ ), they become  $3.7 \times 10^6 \text{ K}$ ,  $7 \times 10^6 \text{ K}$ , and  $1.2 \times 10^8 \text{ K}$ , respectively. The last estimate is virtually equal to  $T_q$ .

In this work, we shall focus on the liquid and gas plasma phase  $\Gamma \leq 175$ . Particular attention will be paid to the very strongly coupled liquid at  $100 \lesssim \Gamma \leq 175$ . In terms of density, we shall limit ourselves to the range  $500 \leq r_s \leq 2400$ . For carbon plasma, this translates into  $11.12 \geq \log_{10} \rho \geq 9.07$ . In Fig. 1, the physical range to be studied is confined by two vertical dotted lines and the melting line.

The range of temperatures and densities addressed in this work covers completely the areas of the relevance strip belonging to domains III, IV, and V (in the liquid phase) and partially covers its portion belonging to domain II. The reaction rates in domains I and II are generally considered known reliably (this will be further confirmed by our results). By contrast, in domains III, IV, and V, the rates are subject to some uncertainties (e.g., Chugunov et al. 2007). Thus, if we manage to calculate the reaction rates in our target temperature and density range, the plasma screening problem in the liquid phase of the OCP will be fully solved [within the framework of Eq. (1)].

## 2 PREVIOUS WORK

Following the original work of Wildhack (1940), Schatzman (1948), and Salpeter (1954), plasma screening of nuclear reactions has been investigated in many excellent papers (see, e.g., Chugunov 2021, for an extensive compilation of these works). Broadly speaking, they can be divided into 3

groups: (i) earlier research, oftentimes semi-analytic, culminating in the paper by Alastuey & Jancovici (1978); (ii) a series of works based on more advanced classic Monte Carlo (MC) simulations including Itoh, Kuwashima & Munakata (1990), Ogata, Iyetomi & Ichimaru (1991), Chugunov et al. (2007); (iii) quantum MC simulations of Ogata (1997) and Militzer & Pollock (2005). For our purposes here, the most important are the quantum calculations of the last group as well as the most recent classic MC based study by Chugunov et al. (2007).

The present paper is devoted to a first-principle calculation of true quantum-mechanical  $g(0)$  by the method of path-integral Monte Carlo (PIMC) simulations. Currently, PIMC is the preferred method for solving quantum many-body problems of this sort. For the first time, this task has been addressed by Ogata (1997), who expressed the ratio of the true  $g(0)$  to its thermonuclear limit via the ratios of ensemble averages of certain Boltzmann exponentials. These averages were evaluated directly with the aid of MC sampling. The range of physical parameters chosen by Ogata intersected the relevance strip. The positions of some of his datapoints are shown by crosses in Fig. 1. For practical applications, Ogata (1997) approximated numerical results by a convenient analytic formula which allows for an easy comparison with any new results. Ogata has shown that it was sufficient to consider distinguishable particles, i.e. the ion statistics played no role. It appears (cf. Fig. 4 of Ogata 1997) that, when sampling exponentials, he had to deal with rather strongly fluctuating quantities.

The only other PIMC calculation of  $g(0)$  has been reported by Militzer & Pollock (2005). It is not 100% clear what method of extracting  $g(0)$  from PIMC simulations was used by these authors. It appears that they extrapolated the numerical values of  $\ln[g(r)]$  from finite  $r > a_i$  which could be sampled in MC runs (close encounters with  $r < a_i$  are exponentially rare due to the Coulomb barrier) to  $r \rightarrow 0$ . Unfortunately, the results of Militzer & Pollock (2005) in the liquid were obtained outside of the relevance strip, at such conditions where  $g(0)$  was relatively big and the burning time was extremely brief, much shorter than 1 second. Four of their points are shown by dots in Fig. 1 while the other 32 points lie outside of the temperature or density ranges spanned by this figure. The authors proposed no way of extrapolating the results into the physically relevant domain and, for this reason, their data cannot be directly compared with ours.

A totally different method was employed by Chugunov et al. (2007). These authors worked with a pair correlation function found in classic MC simulations. Classic  $g(0) = 0$ . However, one can define the effective spherically symmetric pair potential  $U(r)$  according to  $g(r) = \exp[-U(r)/T]$ . This potential contains a divergent Coulomb term and a finite term responsible for screening. The latter was extrapolated to  $r \rightarrow 0$ . Once again, close encounters are extremely rare, thus one has to base the extrapolation on numerical results at  $r > a_i$ . After that, the tunneling probability and respective  $g(0)$  were found via the standard quantum-mechanical WKB technique. The same method was used earlier by Itoh et al. (1990) with similar results. In Chugunov et al. (2007), it was stated that their extrapolated potential was more advanced than that of Itoh et al. (1990). Chugunov et al. (2007) also approximated their numerical results by a rather convenient analytic

formula. We note in passing, that in Line (D) of their Tab. III, when describing the analytic formula of [Ogata \(1997\)](#), [Chugunov et al. \(2007\)](#) omitted a term given by Eq. (22) of [Ogata \(1997\)](#).

One may wonder, whether calculations based on classic MC have a chance of being accurate? In a related problem, calculations of the liquid OCP energy by the PIMC method ([Jones & Ceperley 1996](#); [Baiko 2019](#)) reveal a significant difference with the classic MC energy in the density range  $600 \leq r_s \leq 2400$  relevant for the present work. The discrepancy becomes worse as the system becomes more quantum. Obviously though, the work of [Chugunov et al. \(2007\)](#) is not just classic but takes into account the crucial quantum tunneling effect.

Conversely, one may ask why use an extremely time-consuming PIMC method given the relative ease of classic MC based or semi-analytic treatments? To answer this question, one has to realise that the accuracy of an approach such as that of [Chugunov et al. \(2007\)](#) is, in fact, unknown until it is compared to a first-principle calculation as a number of effects remains unaccounted for. First of all, not a single tunneling event occurs in a static spherically-symmetric potential. The actual potential, produced by many ions, fluctuates in time and space. Even its spherically-symmetric average is likely affected by the quantum nature of surrounding particles and differs from the respective average deduced from classic MC. Each tunneling is a three-dimensional anisotropic process which, in general, cannot be described by a one-dimensional radial WKB formula. Finally, it is not clear whether the extrapolation procedure for  $U(r)$  is unambiguous.

[Chugunov et al. \(2007\)](#) claim that none of these effects is expected to be strong in thermonuclear regime with strong plasma screening (domain II). In domains III, IV, and V, the situation is less optimistic. PIMC allows one to take all these effects into account, provide reliable numerical results in the most problematic parameter range, and quantify the precision of the quasiclassic treatment.

### 3 FORMALISM

#### 3.1 General formula

The pair correlation function at a spatial separation  $\mathbf{r}$  reads (e.g., [Ogata 1997](#))

$$g(\mathbf{r}) = \frac{\Omega \text{Sp} [\delta(\mathbf{r}_{12} - \mathbf{r}) e^{-\beta \mathcal{H}}]}{\text{Sp} [e^{-\beta \mathcal{H}}]}, \quad (2)$$

where  $\Omega$  is the volume, ‘Sp’ means trace,  $\mathcal{H}$  is the system Hamiltonian,  $\beta = 1/T$ ,  $\mathbf{r}_{12} = \mathbf{r}_1 - \mathbf{r}_2$ ,  $\mathbf{r}_j$  is the coordinate of the  $j$ -th particle (i.e. a wave function argument over which one integrates when computing matrix elements),  $j = 1, 2, \dots, N$ . Finally,  $N$  is the total number of particles.

The traces in Eq. (2) can be evaluated in any representation but we shall use the coordinate representation where the quantum numbers are particle coordinates  $\mathbf{R}_1, \mathbf{R}_2, \dots, \mathbf{R}_N$  (over which one integrates when computing trace). A calligraphic  $\mathcal{R} = \{\mathbf{R}_1, \mathbf{R}_2, \dots, \mathbf{R}_N\}$  denotes a full set of these quantum numbers specifying a basis function of the coordinate representation.

In the denominator of Eq. (2), one has the partition func-

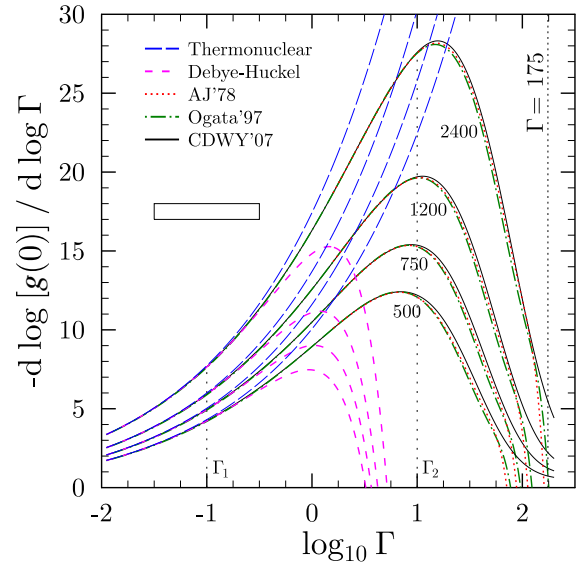


**Figure 2.** Minus the logarithmic derivative of  $g(0)$  with respect to  $\log \Gamma$  in the thermonuclear limit (long-dashed), Debye-Hückel approximation (short-dashed), models of [Alastuey & Jancovici \(1978\)](#) (dotted), [Ogata \(1997\)](#) (dot-dashed), and [Chugunov et al. \(2007\)](#) (solid). The rectangle demonstrates an area under a curve producing a 10-fold change of  $g(0)$  and the respective reaction rates. Numbers near the curves are  $r_s$  values.

tion and the numerator can be expected to behave in a similar way. In simulations, one typically tries to avoid direct computation of the partition function because it involves averaging exponentials which produces excessive fluctuations during sampling (e.g., [Ceperley 1995](#)). Instead, one computes energy, which is a much better behaved quantity, and then integrates it over temperature to obtain the Helmholtz free energy (proportional to the logarithm of the partition function).

Acting in the same spirit let us consider

$$\frac{d}{d\beta} \ln g(\mathbf{r}) = \frac{\text{Sp} [\mathcal{H} e^{-\beta \mathcal{H}}]}{\text{Sp} [e^{-\beta \mathcal{H}}]} - \frac{\text{Sp} [\delta(\mathbf{r}_{12} - \mathbf{r}) \mathcal{H} e^{-\beta \mathcal{H}}]}{\text{Sp} [\delta(\mathbf{r}_{12} - \mathbf{r}) e^{-\beta \mathcal{H}}]}. \quad (3)$$

The method that we outline allows one to find  $g(\mathbf{r})$  at any  $\mathbf{r}$ , but from now on we shall focus on  $g(0)$ . Consequently, we obtain

$$\ln \frac{g(0, \Gamma_2)}{g(0, \Gamma_1)} = \int_{\ln \Gamma_1}^{\ln \Gamma_2} d \ln \Gamma \beta (\langle \mathcal{H} \rangle - \langle \mathcal{H} \rangle_{\mathbf{r}_{12}=0}). \quad (4)$$

In this case,  $\langle \mathcal{H} \rangle$ , given by the first fraction on the right-hand side of Eq. (3), is the ordinary energy of the system, and

$$\langle \mathcal{H} \rangle_{\mathbf{r}_{12}=\mathbf{r}} = \frac{\text{Sp} [\delta(\mathbf{r}_{12} - \mathbf{r}) \mathcal{H} e^{-\beta \mathcal{H}}]}{\text{Sp} [\delta(\mathbf{r}_{12} - \mathbf{r}) e^{-\beta \mathcal{H}}]} \quad (5)$$

is a similar average restricted to functions with  $\mathbf{R}_1 = \mathbf{R}_2 + \mathbf{r}$ . For clarity, we included  $\Gamma$  into the list of arguments of the pair correlation function in Eq. (4). Thus, if the quantity  $\beta (\langle \mathcal{H} \rangle - \langle \mathcal{H} \rangle_{\mathbf{r}_{12}=0})$  is calculated for all  $\Gamma$  greater than some fixed value  $\Gamma_1$ , it can be integrated over  $\ln \Gamma$  to find  $g(0, \Gamma_2)$  at any  $\Gamma_2$  provided  $g(0, \Gamma_1)$  is known.

#### 3.2 Illustration

To get a better feel of this quantity, it is helpful to plot the integrands generating  $g(0)$  via Eq. (4) in already existing mod-

els. In Fig. 2, curves of different types correspond to different models at  $r_s$  values indicated next to them. The area under any curve between any two  $\Gamma$ , say  $\Gamma_1 = 0.1$  and  $\Gamma_2 = 10$  is equal to minus decimal logarithm of the factor by which  $g(0)$  drops from  $\Gamma_1$  to  $\Gamma_2$  in the respective model. For illustration, the rectangle shows an area changing the decimal logarithm by 1. We see, for instance, that the area under the  $r_s = 2400$  curves is much larger than that under the  $r_s = 500$  curves, which means that  $g(0)$  and reaction rates at  $r_s = 2400$  drop much faster than those at  $r_s = 500$  over the same  $\Gamma$ -range.

Long-dashed and short-dashed curves display the thermonuclear and Debye-Hückel limits, respectively. The main qualitative difference between them is the appearance of maxima at  $\Gamma \sim 1$  and descending portions of the curves in the Debye-Hückel model. These features represent the main effect of the ion screening. They prevent an extremely rapid drop of  $g(0)$  with increase of  $\Gamma$  predicted by the pure thermonuclear curves.

However, a comparison with other, more sophisticated, models demonstrates that the importance of ion screening is greatly overestimated by the Debye-Hückel approximation in the liquid regime  $\Gamma > 1$ . Dotted, dot-dashed and solid curves show the results of Alastuey & Jancovici (1978), Ogata (1997), and Chugunov et al. (2007), respectively, and the areas under these curves are obviously bigger than those under the short-dashed curves. Accordingly, the decrease of  $g(0)$  with  $\Gamma$  obtained by these authors is much stronger than in the Debye-Hückel model. The three parametrisations agree with each other relatively well. We do observe some differences between the descending segments of the curves at  $\Gamma \gtrsim 10$ . Most apparent differences occur at  $\Gamma \gtrsim 100$  where the curves of Alastuey & Jancovici (1978) and Ogata (1997) drop to zero. This means that at some point in the liquid phase their  $g(0)$  stop decreasing with decrease of temperature so that the reaction rates become temperature independent. This corresponds to the onset of the pycnonuclear regime V (cf. Section 1) and is qualitatively consistent with the  $T_q$  value above the melting temperature. On the contrary,  $g(0)$  as predicted by Chugunov et al. (2007) continues to decrease (i.e. depends on temperature) all the way down to the crystallisation line  $\Gamma = 175$ .

At low  $\Gamma$ , all models merge which means that  $g(0, \Gamma_1)$  can be taken from the thermonuclear limit at a sufficiently low  $\Gamma_1$ .

### 3.3 PIMC implementation

The energy of a quantum Coulomb liquid  $\langle \mathcal{H} \rangle$  has been recently calculated by the PIMC method (Baiko 2019) and we refer to this work for details of our specific realisation of the method (see also Ceperley 1995; Jones & Ceperley 1996). For both,  $\langle \mathcal{H} \rangle$  and  $\langle \mathcal{H} \rangle_{r_{12}=0}$ , we split  $e^{-\beta \mathcal{H}} = (e^{-\tau \mathcal{H}})^M$ , where  $\tau = \beta/M$ ,  $M$  is a positive integer. In the numerators of Eq. (3), one can commute  $\mathcal{H}$  with an arbitrary number of factors  $e^{-\tau \mathcal{H}}$  which should not affect the result. In what follows, this is referred to as a slice number (or a bead number) selection for an energy estimate.

In view of the Trotter formula

$$e^{-\beta(\mathcal{T}+\mathcal{V})} = \lim_{M \rightarrow \infty} \left[ e^{-\tau \mathcal{T}} e^{-\tau \mathcal{V}} \right]^M \quad (6)$$

(where  $\mathcal{T}$  and  $\mathcal{V}$  are kinetic and potential energy opera-

tors, respectively), one can approximately replace  $e^{-\tau \mathcal{H}} \rightarrow e^{-\tau \mathcal{T}} e^{-\tau \mathcal{V}}$  everywhere. This is known as the primitive approximation (its accuracy should be improving with decrease of  $\tau$  and is further discussed below).

Then one can insert full sets of basis functions  $\mathcal{R}_l = \{\mathcal{R}_1^{(l)}, \mathcal{R}_2^{(l)}, \dots, \mathcal{R}_N^{(l)}\}$  between all operators in Eq. (3) ( $l$  enumerates basis sets). Any matrix elements of  $e^{-\tau \mathcal{T}}$  and  $e^{-\tau \mathcal{V}}$  can be easily evaluated analytically in the coordinate representation (e.g., Ceperley 1995). For instance,

$$\begin{aligned} & \int d\mathcal{R} \langle \mathcal{R}_1 | e^{-\tau \mathcal{T}} | \mathcal{R} \rangle \langle \mathcal{R} | e^{-\tau \mathcal{V}} | \mathcal{R}_2 \rangle \\ &= \int \frac{d\mathcal{R}}{(4\pi\lambda\tau)^{3N/2}} \exp \left[ -\frac{(\mathcal{R}_1 - \mathcal{R})^2}{4\lambda\tau} \right] e^{-\tau V(\mathcal{R})} \delta(\mathcal{R} - \mathcal{R}_2) \\ &= \frac{1}{(4\pi\lambda\tau)^{3N/2}} \exp \left[ -\frac{(\mathcal{R}_1 - \mathcal{R}_2)^2}{4\lambda\tau} - \tau V(\mathcal{R}_2) \right], \quad (7) \end{aligned}$$

where  $\lambda = \hbar^2/(2m_i)$  and  $V(\mathcal{R})$  is the system potential energy when ion coordinates are equal to  $\mathcal{R}$ . A matrix element of the Hamiltonian between these basis functions in Eq. (3) can be also readily derived which yields an expression called an *energy estimator*.

After some algebra, one is left with  $M+1$  basis functions  $\mathcal{R}_0, \mathcal{R}_1, \dots, \mathcal{R}_M$ ,  $\mathcal{R}_0 = \mathcal{R}_M$  being final and initial states equal to each other because we calculate trace. Functions  $\mathcal{R}_1, \mathcal{R}_2, \dots, \mathcal{R}_{M-1}$  describe intermediate states. We denote the energy estimator as  $H(\mathcal{R}_m)$  where  $m$  (which can take values 1, 2,  $\dots, M-1$ ) is the slice number selected for the energy estimate. A lengthy explicit formula for  $H(\mathcal{R}_m)$  can be found, e.g., in Eq. (6.5) of Ceperley (1995).

Combining the above formulae, one obtains

$$\begin{aligned} \langle \mathcal{H} \rangle &= \int d\sigma \pi(\sigma) H(\mathcal{R}_m), \quad (8) \\ \langle \mathcal{H} \rangle_{r_{12}=0} &= \int d\sigma_0 \pi_0(\sigma_0) H(\mathcal{R}_m), \\ \pi(\sigma) &= \frac{1}{Z} \exp \left[ -\sum_{l=1}^M S_l \right], \\ e^{-S_l} &= \frac{1}{(4\pi\lambda\tau)^{3N/2}} \exp \left[ -\frac{(\mathcal{R}_l - \mathcal{R}_{l-1})^2}{4\lambda\tau} - \tau V(\mathcal{R}_l) \right] \\ \sigma &= \{\mathcal{R}_1, \mathcal{R}_2, \dots, \mathcal{R}_M = \mathcal{R}_0\}. \end{aligned}$$

In this case,  $\sigma$  is the  $3NM$ -dimensional domain of quantum numbers (coordinates of  $N$  ions in all  $M$  states) and  $\pi(\sigma)$  is a product of matrix elements of the operator exponentials. Since  $\pi(\sigma)$  is strictly positive, while  $Z$  [coming from the denominator in Eq. (3)] ensures that  $\pi(\sigma)$  is normalized to 1, it is natural to interpret  $\pi(\sigma)$  as a probability distribution, and the task of finding  $\langle \mathcal{H} \rangle$  reduces to averaging the energy estimator with it.

The  $3(NM-1)$ -dimensional domain  $\sigma_0$  differs from  $\sigma$  in that coordinates of particles 1 and 2 in the initial and final states always coincide:  $\mathcal{R}_1^{(0)} = \mathcal{R}_2^{(0)}$ . The distribution  $\pi_0(\sigma_0)$  is then obtained from  $\pi(\sigma)$  by a straightforward modification of the kinetic energy terms in  $e^{-S_1}$  and  $e^{-S_M}$ . In the potential energy, the singular exponential does not enter  $\pi_0$  because it is simply a common factor (for any finite  $\mathbf{r}$ , it is  $\sim e^{-\tau Z_i^2 e^2/|\mathbf{r}|}$ ) which cancels out with the denominator.

As is well known (e.g., Ceperley 1995), the quantum system at finite  $M$  is isomorphic to a system of  $N$  classic ring polymers each with  $M$  beads. The bead coordinates of the

$j$ -th ring are of course  $\mathbf{R}_j^{(0)}, \mathbf{R}_j^{(1)}, \dots, \mathbf{R}_j^{(M)} = \mathbf{R}_j^{(0)}$ . In order to find the average energy  $\langle \mathcal{H} \rangle$ , one studies a system of  $N$  independent polymers. To calculate  $\langle \mathcal{H} \rangle_{r_{12}=0}$ , the ring polymers describing particles 1 and 2 have a common zeroth bead of double mass and double charge.

Sampling is done with the aid of the Metropolis algorithm. We attempt two move types, single bead moves and whole polymer moves. The details can be found in [Baiko \(2019\)](#).

Since we are now interested in a relatively small difference of two close quantities:  $\langle \mathcal{H} \rangle - \langle \mathcal{H} \rangle_{r_{12}=0}$ , where each of the averages can be extracted from simulations with appreciable errors, it is desirable to work in such a way that would result in a cancellation of common sources of variance. In a sense, it is the same principle as that governing differential amplifiers very popular in electrotechnics: common mode noises cancel but the difference between two inputs is amplified. In order to achieve this, we run simulations for  $\langle \mathcal{H} \rangle$  and  $\langle \mathcal{H} \rangle_{r_{12}=0}$  in parallel with identical random sequences and the same initial conditions, except that, for  $\langle \mathcal{H} \rangle_{r_{12}=0}$ , we find two particles in the initial file with the smallest separation between them, shift the particles towards the mid-point positioning them very close to each other and merge their zeroth beads right at the mid-point. Furthermore, we use the same slice  $m$  for energy estimates, same estimator (see below) and perform the estimates after the same number of attempted moves of the Metropolis process.

Let us add a few more words regarding the slice number  $m$  and estimator selection for the energy estimates. For  $\langle \mathcal{H} \rangle_{r_{12}=0}$ , the *thermodynamic* estimator [e.g., Eq. (6.7) of [Ceperley \(1995\)](#)] shows very pronounced slice-number dependence, because it relies on equivalence of beads. But they are no longer equivalent in the  $\langle \mathcal{H} \rangle_{r_{12}=0}$  simulation being closer or further away from the common bead. Simply put, the thermodynamic estimator is not appropriate here.

Instead, one should use the *direct* or *Hamiltonian* energy estimator [e.g., Eq. (6.5) of [Ceperley \(1995\)](#)], which is just the matrix element  $H(\mathcal{R}_m)$  introduced above. This estimator turns out to be much closer to being  $m$ -independent. It has an extended  $m$ -independent ‘shelf’ at intermediate  $m$ , yet, there is a noticeable  $m$ -dependence for several slices near the common bead. The reason for this (unwanted)  $m$ -dependence of the direct estimator for  $\langle \mathcal{H} \rangle_{r_{12}=0}$  is related to the fact that the accuracy of the primitive approximation  $e^{-\tau \mathcal{H}} \rightarrow e^{-\tau \mathcal{T}} e^{-\tau \mathcal{V}}$  is not uniform across slices. It can be expected to be worse for  $m$  near the common bead because  $\mathcal{V}$  is relatively large there.

An analysis shows that, if one compares, for instance,  $m = 2$  for a particular  $\tau$  and  $m = 4$  for a two times smaller  $\tau$  (i.e. two times greater  $M$ ), the energy estimate will be closer to the shelf in the second case. In other words, with increase of  $M$ , the shelf widens (in imaginary time) towards the common bead. As far as  $\langle \mathcal{H} \rangle$  is concerned, there is no dependence on  $m$  regardless of which energy estimator (direct or thermodynamic) is used and both estimators, within statistical errors, yield the same result. This leads us to a procedure where for  $\langle \mathcal{H} \rangle_{r_{12}=0}$  we employ the direct estimator with  $m$  taken at least 5–6 beads away from the common bead, i.e. on the shelf, and the same  $m$  and the estimator are chosen for  $\langle \mathcal{H} \rangle$ .

The primitive approximation becomes exact as  $M \rightarrow \infty$ . In practice, one can perform calculations at several  $M$  and then extrapolate to  $1/M \rightarrow 0$ . Such an approach is used for calculation of liquid and crystal energies ([Baiko 2019](#), [Baiko](#)

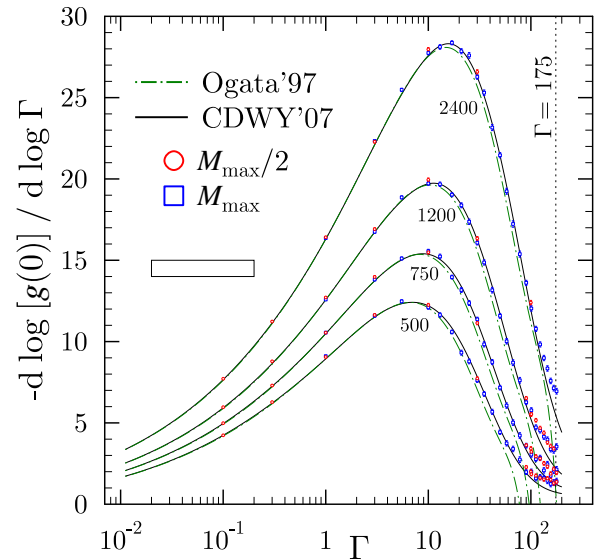


**Figure 3.** Simulation results for the integrand of Eq. (4) for a maximum number of beads (squares) and for two times fewer beads (circles). The other curves are the same as in Fig. 2.

& Chugunov, submitted). In the present problem though, the difference  $\langle \mathcal{H} \rangle - \langle \mathcal{H} \rangle_{r_{12}=0}$  has no observable  $M$ -dependence for sufficiently large  $M$  (cf. Figs. 3 and 4). This is likely related to a good cancellation of  $M$ -dependent terms in the two averages. The same effect has been also observed earlier by [Ogata \(1997\)](#).

Any first principle simulation is performed with a finite number of particles ( $N = 250$  in our case) and there is always the question whether the results are sensitive to  $N$  and what would they be in the thermodynamic limit? The only way to conclusively answer this question is to perform simulations at several  $N$  and analyse the ensuing  $N$ -dependence. This program requires extra resources and has not been implemented within the framework of this paper. We note, however, that [Ogata \(1997\)](#) has reported calculations at two values of  $N = 50$  and  $100$  and found no substantial  $N$ -dependence.

## 4 RESULTS

In Fig. 3, we present results of our simulations (as one-sigma bars) for  $r_s = 500, 750, 1200$  and  $2400$ , along with the integrands derived from the analytic fits of [Ogata \(1997\)](#) (dot-dashed) and [Chugunov et al. \(2007\)](#) (solid). These curves have already been displayed in Fig. 2. Squares correspond to a maximum number of beads in a ring polymer achieved in simulations, circles are for two times fewer beads.

We would like to emphasize that the methods and calculations, compared in Fig. 3, are completely independent. In our approach, there is no reference to classic ion plasma, its pair correlation function or free energy. Tunneling is not treated as a separate, factored-out process. Nevertheless, the excellent agreement from the thermonuclear limit up to  $\Gamma \sim 10$  mutually validates different theoretical approaches. The thermonuclear limit itself is verified by our numerical results at low  $\Gamma$ .

On the descending portions of the curves our data favor

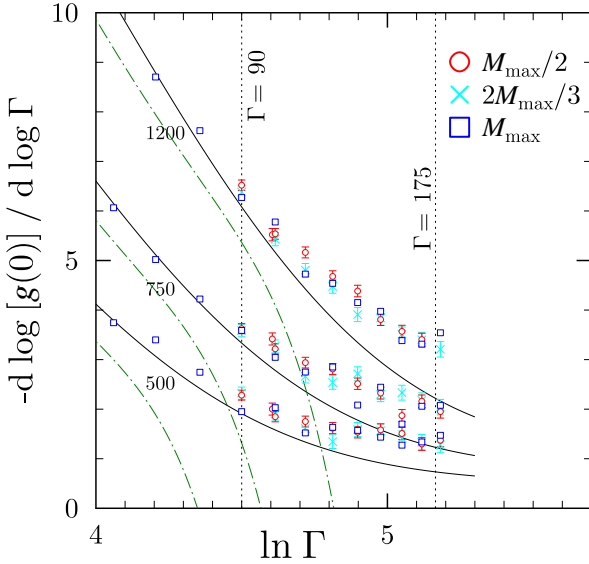


**Figure 4.** Zoomed-in high- $\Gamma$  area of Fig. 3. Also shown are calculations at an intermediate number of beads (crosses).

the parametrisation of Chugunov et al. (2007). However, at  $\Gamma \gtrsim 100$ , our points deviate from their curves and predict somewhat smaller  $g(0)$  and slower reaction rates (cf. Fig. 6). Importantly, our data confirm that the integrands do not drop to zero in the liquid phase and the reaction rates continue to depend on  $T$  at least down to the crystallisation (cf. Fig. 4).

Let us note, that different  $r_s$  and  $\Gamma$  points have been calculated by PIMC using different random sequences, initial conditions, numbers of MC steps, slice numbers at which the energy was estimated. This explains a higher variance *between* our datapoints than may have been expected based on the error bar sizes characterising individual MC runs.

A comparison of squares and circles does not reveal any systematic dependence of our results on  $M$ . A few misses at various  $r_s$  and  $\Gamma$  should be attributed to fluctuations. This point is illustrated further in Fig. 4 where we consider the  $\Gamma \gtrsim 100$  region in more detail. Solid curves represent analytic fits of Chugunov et al. (2007). Symbols show simulation results at three different  $M$  whose inverse values are evenly spaced. Squares and circles are the same data as in Fig. 3. In the case of squares, we omit the error bars to improve the graph readability. They are of about the same size as the drawn bars. Crosses correspond to an intermediate number of beads. Basically, this figure demonstrates that the  $M$ -dependence has already saturated in the considered  $M$ -range, and the results at the maximum number of beads can be used as the ‘production’ datapoints. Dot-dashed curves are fits of Ogata (1997) which are clearly in a serious disagreement with our calculations in this  $\Gamma$ -range.

In Fig. 5, we show the final dataset. Calculations were performed at 6 values of  $r_s$  and multiple values of  $\Gamma$  in order to sample as best as practicable the deviation from the analytic parametrisation of Chugunov et al. (2007) plotted by the dotted curves. Different colours serve to highlight data groups sharing the same  $r_s$ . The solid curves provide an analytic fit to the PIMC data. They are obtained by adding a simple expression,  $10^{-6}\Gamma^2\sqrt{r_s}$ , to the dotted curves.

This expression can be easily integrated over  $\ln \Gamma$  to yield

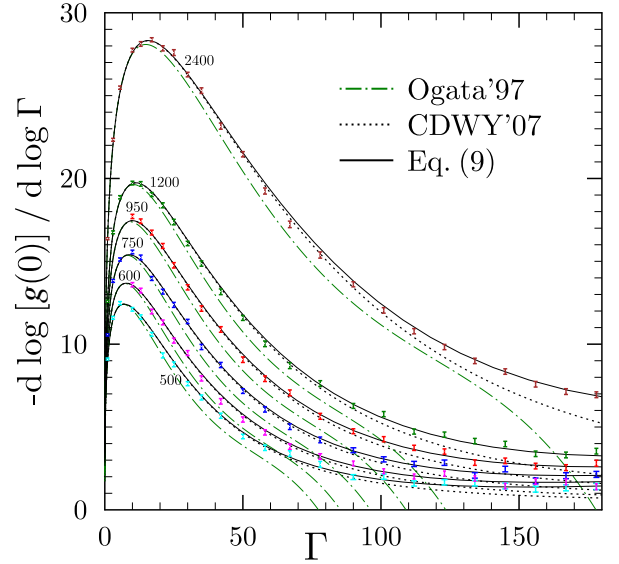


**Figure 5.** Bars show the present PIMC results at the maximum number of beads. Colours highlight the data with the same  $r_s$ . Dotted, dot-dashed, and solid curves are the parametrisation of Chugunov et al. (2007), Ogata (1997), and the fit, Eq. (9), respectively, at  $r_s$  values indicated near the curves.

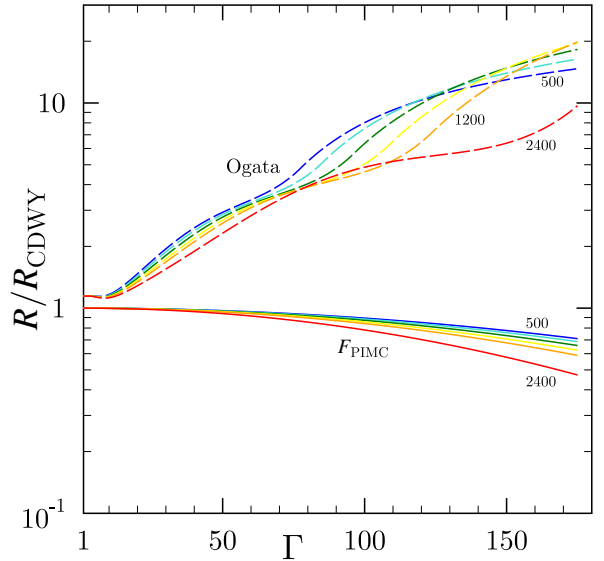


**Figure 6.** The ratios of the reaction rates,  $R$ , as reported by Ogata (1997) (dashes) and calculated in the present work (solid curves) to those due to Chugunov et al. (2007), denoted as  $R_{\text{CDWY}}$ . Numbers near the curves are the respective  $r_s$  values.

a correction to  $g(0)$  of Chugunov et al. (2007):

$$g_{\text{PIMC}}(0) = g_{\text{CDWY}}(0)F_{\text{PIMC}}, \quad (9)$$

$$F_{\text{PIMC}} = \exp[-5 \times 10^{-7}\Gamma^2\sqrt{r_s}].$$

In this case,  $g_{\text{PIMC}}(0)$  is our final result for the ion pair correlation function at zero separation. The respective modification of the reaction rates is depicted in Fig. 6. The ratios of the reaction rates to those reported by Chugunov et al. (2007) are plotted as functions of  $\Gamma$  for  $r_s = 500, 600, 750, 950, 1200$  and  $2400$ . The lower group of curves shows the present results while the upper group of curves displays the predictions of Ogata (1997). We conclude that in

the physically relevant range of temperatures and densities, [Chugunov et al. \(2007\)](#) overestimate the reaction rates by no more than a factor of two whereas rates of [Ogata \(1997\)](#) are overestimated by up to a factor of 30.

In the process of working on this paper we have calculated anew the energies of quantum liquid OCP in the density range  $500 \leq r_s \leq 2400$  which turned out to be in a very good agreement with the earlier computation and fit ([Baiko 2019](#); [Baiko & Yakovlev 2019](#)). This development will be reported in more detail elsewhere ([Baiko & Chugunov, submitted](#)).

## 5 CONCLUSION

A first-principle method to calculate the ion pair correlation function and plasma screening factor in a Coulomb plasma is developed. The method is applied for an analysis of nuclear reaction rates in a practically relevant range of temperatures and densities typical for liquid layers of white dwarf cores and neutron star crusts. It is shown that among the earlier results on ion screening the most accurate are those of [Chugunov, DeWitt & Yakovlev \(2007\)](#). Nevertheless, at  $\Gamma \gtrsim 100$  a deviation of screening factors from analytic fits of these authors is discovered which implies a reduction of the reaction rates by up to a factor of two. A simple formula is proposed to fit the respective correction to the reaction rates valid for all  $\Gamma$  and  $r_s$  in the studied range.

The developed method can be extended to the case of crystallised phase of stellar matter as well as to ionic mixtures of various elements which can be present simultaneously in stellar matter undergoing burning (e.g., carbon and helium). In these systems, currently existing theoretical uncertainty of the rates is higher than in the one-component liquid plasma considered here.

Another possible extension of the method could be to take into account the electron screening in a self-consistent manner. As long as the electron screening can be viewed as static, this reduces to a modification of the inter-ion potential. However, it is not straightforward, because such a potential should not be described by the simple Thomas-Fermi screening model ([Potekhin & Chabrier 2013](#)). A more realistic electron dielectric function and potential would have to be used which may significantly slow down the simulations. Currently, the electron screening of nuclear reactions is taken into account on the basis of the free energy difference in a classic ion plasma with *polarisable* background.

A reliable description of nuclear fusion reactions in the liquid phase of stellar matter is important for self-consistent modelling of various astrophysical phenomena involving accretion onto a compact star or a merger of such stars. A local density increase results in an intensification of reactions in a matter element, an energy release, possible melting, and further intensification of reactions. Reconstructing the exact dynamics of this process is crucial for a realistic description of such spectacular transient phenomena as bursts, superbursts, and even Supernovae Ia.

## ACKNOWLEDGEMENTS

The author is sincerely grateful to D. G. Yakovlev for providing numerical data for Fig. 1, reading the manuscript, and valuable comments.

## DATA AVAILABILITY

The data underlying this article will be shared on reasonable request to the corresponding author.

## REFERENCES

- Alastuey A., Jancovici B., 1978, *ApJ*, 226, 1034  
 Baiko D. A., 2019, *MNRAS*, 488, 5042  
 Baiko D. A., Yakovlev D. G., 2019, *MNRAS*, 490, 5839  
 Beard M., Afanasjev A. V., Chamon L. C., Gasques L. R., Wiescher M., Yakovlev D. G., 2010, *At. Data Nucl. Data Tables*, 96, 541  
 Brown L. S., Sawyer R. F., 1997, *Rev. Mod. Phys.*, 69, 411  
 Ceperley D. M., 1995, *Rev. Mod. Phys.*, 67, 279  
 Chugunov A. I., 2021, *J. Phys.: Conf. S.*, 1787, 012047  
 Chugunov A. I., DeWitt H. E., 2009, *Phys. Rev. C*, 80, 014611;  
 Chugunov A. I., DeWitt H. E., 2009, *Contrib. Plasm. Phys.*, 49, 696  
 Chugunov A. I., DeWitt H. E., Yakovlev D. G., 2007, *Phys. Rev. D*, 76, 025028  
 Clayton D. D., 1983, *Principles of Stellar Evolution and Nucleosynthesis* (Chicago: Univ. Chicago Press)  
 Haensel P., Potekhin A. Y., Yakovlev D. G., 2007, *Neutron Stars. 1. Equation of State and Structure* (Springer, New York)  
 Ichimaru S., 1993, *Rev. Mod. Phys.*, 65, 255  
 in 't Zand J., 2017, in Serino M. et al., eds, 7 years of MAXI: Monitoring X-ray Transients. Wako, Saitama, Japan. p. 121  
 Itoh N., Kuwashima F., Munakata H., 1990, *ApJ*, 362, 620  
 Jeffery C. S., Karakas A. I., Saio H., 2011, *MNRAS*, 414, 3599  
 Jones M. D., Ceperley D. M., 1996, *Phys. Rev. Lett.*, 76, 4572  
 Militzer B., Pollock E. L., 2005, *Phys. Rev. B*, 71, 134303  
 Ogata S., 1997, *ApJ*, 481, 883  
 Ogata S., Iyetomi H., Ichimaru S., 1991, *ApJ*, 372, 259  
 Parikh A., José J., Sala G., 2014, *AIP Advances*, 4, 041002  
 Potekhin A. Y., Chabrier G., 2013, *Contrib. Plasm. Phys.*, 53, 397  
 Ruiter A. J., 2020, in Barstow M. A. et al., eds, *Proc. IAU Symp.* 357, *White Dwarfs as Probes of Fundamental Physics: Tracers of Planetary, Stellar and Galactic Evolution*. p. 1  
 Salpeter E. E., 1954, *Australian J. Phys.*, 7, 373  
 Salpeter E. E., Van Horn H. M., 1969, *ApJ*, 155, 183  
 Sawyer R. F., 2010, *Phys. Rev. Lett.*, 104, 191103  
 Shchechilin N. N., Gusakov M. E., Chugunov A. I., 2021, preprint (arXiv:2105.01991)  
 Schatzman E., 1948, *J. Phys. Rad.*, 9, 46  
 Soker N., 2019, *New Astron. Rev.*, 87, 101535  
 Yakovlev D. G., Shalybkov D. A., 1989, *Sov. Sci. Rev., Ser. E: Astrophys. Space Phys.*, 7, 311  
 Wildhack W. A., 1940, *Phys. Rev.*, 57, 81